

## Reverse Roll Coating Flow with Non-Newtonian Fluids

Jiin-Yuh Jang\* and Peng-Yuan Chen

*Department of Mechanical Engineering, National Cheng-Kung University, Tainan, 70101 Taiwan.*

Received 4 June 2008; Accepted (in revised version) 6 November 2008

Available online 6 February 2009

---

**Abstract.** In this study an incompressible flow with non-Newtonian fluids in the reverse roll coating process was investigated. Non-Newtonian behavior of the coating fluid was accounted by using power law model with power index,  $n$ , ranging from 0.8 to 1.2. Effect of roll speed ratio ( $V_2/V_1$ ) of the panel roll to the applicator roll and gap distance on the coating film thickness were also investigated. Numerical results were in good agreement with those of experimental data within 15%-20%. Results indicated that the film thickness ratios are function of power-law index, roll speed ration and ratio of roll radius to gap distance. The equations for film thickness ratio were obtained from numerical results as shown below:

$$\frac{t_2}{t_1} = 0.89n^{0.55} \left(\frac{V_2}{V_1}\right)^{-0.83} \left(\frac{H_0}{R_m}\right)^{0.0025}, \quad \frac{t_3}{t_1} = 65.6n^{0.0014} \left(\frac{V_2}{V_1}\right)^{-0.043} \left(\frac{H_0}{R_m}\right)^{0.624},$$

where  $t_1$ ,  $t_2$  and  $t_3$  are inlet film, transferred film and leakage film thickness, respectively,  $n$  is power-law index,  $V_1$  and  $V_2$  are roll speed of applicator roll and panel roll,  $R_m$  is average radius of two rolls and  $H_0$  is gap distance. The correlations are accurate within 10% for  $0.8 \leq n \leq 1.2$ ,  $0.5 \leq V_2/V_1 \leq 2$ , and  $7.7 \times 10^{-5} \leq H_0/R_m \leq 1.54 \times 10^{-4}$ .

**AMS subject classifications:** 76A05

**Key words:** Reverse roll coating, non-Newtonian flow, power-law.

---

## 1 Introduction

Roll coating is a process by which a thin liquid film is formed on a continuous web or substrate by the use of two or more rotating rolls. This process can be used to produce a wide variety of finishing products. The nip distance between the two rotating rolls is much smaller than the rolls radii and when a fluid flows through such a small gap, it

---

\*Corresponding author. *Email addresses:* jangjim@mail.ncku.edu.tw (J.-Y. Jang), n1891114@mail.ncku.edu.tw (P.-Y. Chen)

comes out as small liquid film, which can be used to coat on a surface. The fluid flow in a small gap between a pair of rotating rolls is the primary factor controlling the thickness and uniformity of the coated film. The thickness of the coating depends primarily on the gap between adjacent rolls and their relative speeds. Depending upon the direction of rolls, roll coating is classified as forward roll coating and reverse roll coating. In forward roll coating, the roll surfaces move in the same direction and in reverse roll coating they move in opposite direction.

Reverse roll coating is an important and common industrial technique widely used to coat magnetic media, adhesive tape, films, foils and coated paper [1,2]. Great advantage of a reverse roll coater is its ability to produce uniform wet films as thin as  $25\ \mu\text{m}$  or less at speeds of up to 5 m/s. The liquid may be Newtonian, but more often it is not; such as is the case for adhesives, paints, or magnetic suspensions. It is also capable of handling liquids of a wide range of viscosity. This makes it an important method of high-speed precision coating.

Over the past five decades, extensive investigations have been carried out to address the flow problems of roll coating processes through experimental, analytical and computational approaches. Early works on reverse roll coating were reported by Ho and Holland [3] and Greener and Middleman [4]. They used lubrication theory to investigate reverse roll coating systems, ignoring the effects of surface tension, the presence of free surfaces and dynamic contact lines. Coyle *et al.* [5] presented a detailed theoretical analysis, along with supporting experiments, which together provide a good description of the operation of a reverse roll coater. The flow in the metering gap of a reverse roll coater was examined by finite element solutions of the Navier-Stokes equations. The results showed that at high speed ratios and capillary numbers, the metered film flow deviated strongly from predictions of lubrication theory. The wetting line moves through the gap center and the metered film thickness passed through a minimum.

Coyle *et al.* [6] presented a simple model of reverse roll coating considering the fluid dynamics of coating flow. The results indicated that the film-transfer free surface and the recirculation under it did not significantly influence the flow rate through the gap. Deviations from lubrication theory occurred only under conditions of low speed ratio and large gap when the effect of gravity became appreciable. Hao and Haber [7] continued the work to study wide ranges of operating conditions that were of practical importance. They used the Galerkin finite element method of solution formulated by Coyle *et al.* [6] to analyze the coating flow problem.

Chandio and Webster [8,9] used finite element modeling to predict the flow associated with the reverse roller-coating of alloy sheets using a protective film of solvent-based lacquer. A finite element simulation of the roller-coating process was presented, based on a semi-implicit Taylor-Galerkin/Pressure-correction algorithm. A mathematical model was derived to describe the solvent coating applied to the underside of the sheet, assuming that the lacquer is a Newtonian fluid. The effects of increasing foil and roll-speeds on characteristic flow quantities such as pressure, lift, drag and shear-rate were reported. At increasing roll-speeds, pressure and lift on the foil display a linear decreasing trend;

the levels of maximum field pressure broaden away from the nip and the location of maximum shear-rate shifts towards the roller.

The non-Newtonian rheological behavior of a coating fluid can strongly affect both the steady, uniform flow and the instabilities of reverse roll coating to which it is susceptible. Coyle *et al.* [10] investigated the flow rate through the gap and the meniscus stability in a reverse roll metering gap, using simple dilute polymer solutions which behave as non-Newtonian liquids. Experiments were conducted with liquids that were shear-thinning but relatively inelastic. Dilute solutions of sodium alginate (Kelcosol) in glycerin (or corn syrup) and tap water were the liquids used. Comparisons of experimental results were made with theoretical predictions based on a Carreau viscosity equation. Experiments with liquids that were markedly elastic were also described, with particular attention paid to flow rate and cascade. Tiu *et al.* [11] experimentally studied the effects of non-Newtonian fluid properties on pre-metered reverse roll coating. A variety of coating liquids exhibiting different rheological properties and surface tensions were formulated for the coating experiments. In the hard/hard roll coating, viscosity is the dominant factor in determining the stripped film on the metering roll; whereas the thickness of the metered film on the applicator roll is dependent only on the liquid feed rate and the roller gap space. In the hard/deformable roll coating, there exists a critical gap space below which the elasto-hydrodynamic interaction between the deformable surface and liquid properties becomes important.

The foregoing extensive literature review shows that there is no substantial work on reverse roll coating process with non-Newtonian flow behavior of coating fluid to date. In this work, the analysis of reverse roll coating with non-Newtonian coating fluid has been carried numerically using finite volume method. Experiments were also conducted on a laboratory roll coater to verify the physical model and numerical accuracy for the complex reverse roll coating process.

## 2 Mathematical analysis

A simple sketch of the reverse roll coating system under the investigation is shown in Fig. 1. The reverse roll coating system consists of two equal radii rolls of 150mm and a big roll of 500mm radius. The 2-D incompressible, isothermal, non-Newtonian laminar flow of liquid in the forming zone of the coated liquid film is considered. The system of governing equations in the absence of body forces for non-conservative form can be expressed as

1. Conservation of Mass :

$$\nabla \cdot \vec{u} = 0. \quad (2.1)$$

2. Conservation of Momentum

$$\rho \frac{\partial \vec{u}}{\partial \tau} + \rho (\vec{u} \cdot \nabla) \vec{u} = \rho \vec{g} - \nabla P + \nabla \cdot (\mu \nabla \vec{u}), \quad (2.2)$$

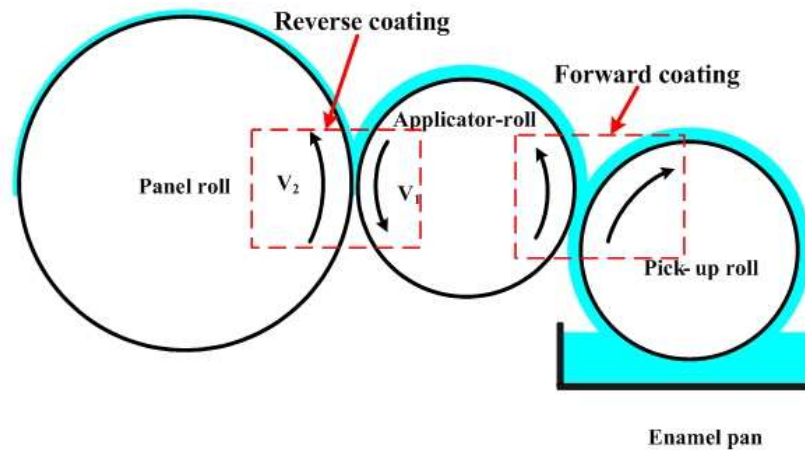


Figure 1: A simple sketch of forward and reverse rolls coating system.

where  $\rho$  is the fluid density,  $\mu$  is the fluid viscosity,  $u$  is the fluid velocity and  $P$  is the fluid pressure. Terms representing the effect of gravity are also omitted for simplicity since their influence is small except at the lowest speeds of rotations and for larger gap widths.

Normally the majority of industrially significant coating liquids exhibit one or other form of non-Newtonian flow behavior namely shear thinning, dilatancy, or viscoelasticity. Coating liquids are commonly suspensions of mineral pigments, solutions of dissolved polymers, or combinations of both. In the present investigation, a mixture of polymer powder is used as coating liquid. For non-Newtonian fluid, the viscosity field varies with local shear rate and can be established simply by means of a power-law equation [12].

$$\mu = \mu_0 (\dot{\gamma}_0)^{1-n} (\dot{\gamma})^{n-1}, \quad (2.3)$$

where  $\mu_0$  is the zero shear rate viscosity,  $\dot{\gamma}_0$  is reference shear rate,  $\dot{\gamma}$  is local calculated shear rate, and  $n$  is the power-law index. The fluid behavior can be classified as pseudoplastic fluid, Newtonian fluid and dilatant fluid based on the value of  $n$ . If  $n < 1$ , the fluid is termed as pseudoplastic or shear-thinning fluid and if  $n > 1$ , the fluid is classified as dilatant or shear-thickening fluid. For a Newtonian fluid,  $n = 1$  and these Newtonian fluids have constant viscosity at all shear rates. Shear thinning fluids have a lower apparent viscosity at higher shear rates and are usually solutions of large, polymeric molecules in a solvent with smaller molecules. Shear thickening fluids have higher apparent viscosity at higher shear rates.

The variation of the apparent viscosity with the shear rate for the present test fluid as shown in Fig. 2 was obtained by a rotating-cylinder viscometer. It is seen that the present test fluid can be modeled approximately as a power law index  $n = 0.95$ . The physical properties of the coating fluid are given below:

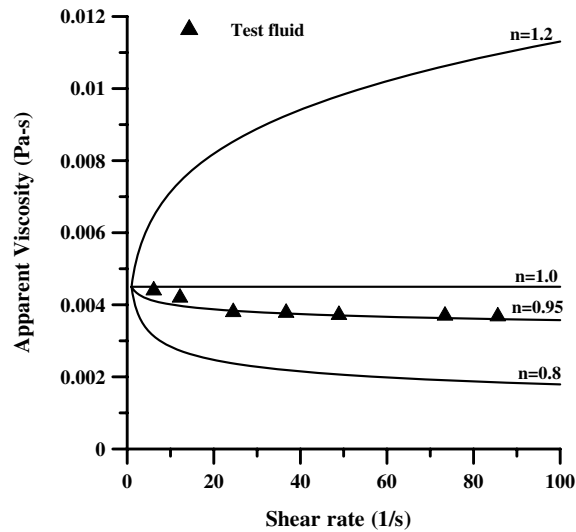


Figure 2: The variation of the apparent viscosity with the shear rate for the test fluid.

Surface tension,  $\sigma = 0.028 \text{ N/m}$ .

The zero shear rate viscosity,  $\mu_0 = 4.5 \times 10^{-3} \text{ Pa-s} = 4.5 \text{ mPa-s}$ .

Density,  $\rho = 1180 \text{ kg/m}^3$ .

Coating flows typically represent the free surface flows. It is essential to predict the location of free surface, which is unknown a priori. In order to fully analyze the roll coating process and to determine the fluid splitting point, the free surface location can be tracked using volume of fluid (VOF) technique [13] by solving the following equation

$$\frac{\partial F}{\partial t} + V \cdot \nabla F = 0, \quad (2.4)$$

$$\bar{\psi} = F\psi_2 + (1-F)\psi_1, \quad (2.5)$$

where  $F$  is a volume fraction and lies between 0 and 1. For  $F = 0$ , the flow domain is assumed to be occupied by air only and for  $F = 1$ , the flow domain is occupied fully by coating liquid. The position of free surface is in some location for which  $0 < F < 1$ .  $\bar{\psi}$  is the volume-averaged property,  $\psi_1$  and  $\psi_2$  are the air and coating fluid properties.

The computational domain used in numerical simulations is shown in Fig. 3. Since the governing equations are elliptic in spatial coordinates, it is necessary to impose boundary conditions at all of the computational domain boundaries (See Fig. 4). At the inlet and outlet area, the pressure was fixed at 1 atm (zero gauge pressure) and the volume fraction  $F$  was assumed to be 1 and 0, respectively. At the solid surfaces, no-slip conditions for velocity are specified. The cyclic boundary conditions were applied on both sides of

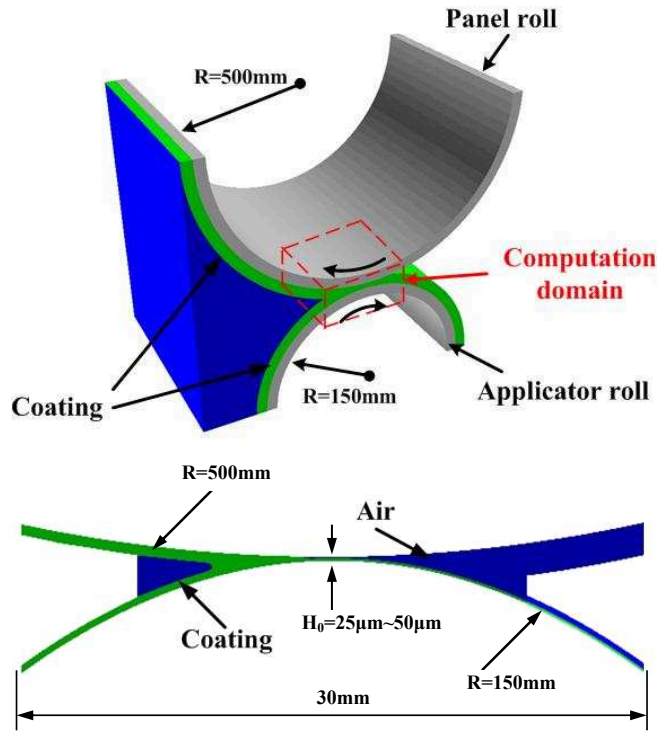


Figure 3: Computational domain used in numerical simulations.

the  $z$ -axis. At free surface i.e. interface between the coating fluid and air the following equilibrium condition between normal stress and the capillary pressure is also applied:

$$N \cdot \overline{\overline{T}} = \frac{1}{Ca} \frac{dt}{ds} - N \cdot P_a, \quad (2.6)$$

where  $\overline{\overline{T}}$  is the stress tensor in fluid,  $N$  and  $t$  are the normal and tangential components of the unit vector to the boundary surface respectively.  $s$  is the arc length along the free surface. The dimensionless Capillary number  $Ca$  is given by the equation

$$Ca = \mu V_1 / \sigma, \quad (2.7)$$

where  $\mu$  and  $\sigma$  are viscosity and surface tension of the coating fluid,  $V_1$  is the applicator roll surface speed.

### 3 Numerical method of solution

The reverse roll coating flow was analyzed by solving Navier-Stokes equations coupled with VOF (Volume of Fluid) technique to track the free surface location. Flow and VOF

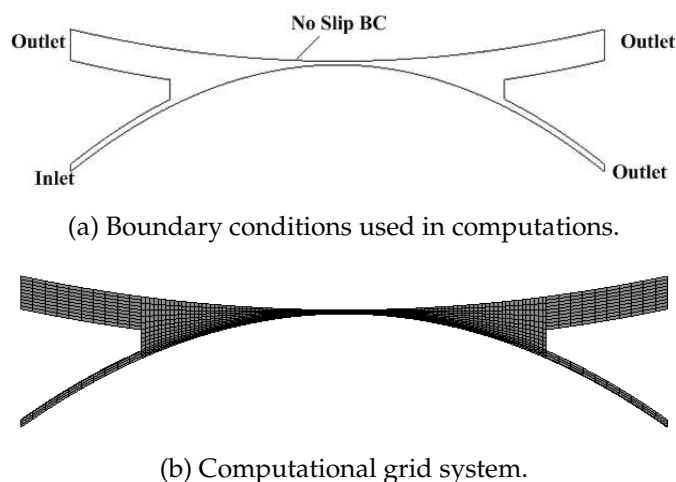


Figure 4: Boundary conditions used in computations and computational grid system.

scheme are used in the analysis to simulate the free surface profile, coating film thickness and the location of the film spitting point of the coating flow between two rollers. In this study, a body-fitted coordinate system along with a multi-block system was used to generate a general curvilinear coordinate system numerically by solving Laplace equations with proper control of grid densities. The governing equations are solved numerically using a control-volume-based finite-difference formulation. The SIMPLEC [14] algorithm is used to solve the system of finite-volume equation iteratively.

The finite volume grid system is shown in Fig. 4. Mesh refinement tests were performed to ensure that the results were independent of the mesh size. A typical grid system with 10,251 grid points is adopted in the numerical computations. A careful check for the grid-independence of the numerical solutions is made to ensure the accuracy of the numerical results. Other three grid systems with 3,926, 15,311 and 18,361 grid points are tested for this purpose. It is found that with the grid system of 10,251 and 15,311 grid points, the relative errors comparing with 18,361 grid points system for the coating film system thickness value at roll speed ratio of 1 are 4.7% and 3.1%, respectively. The coarse grid system with 3,926 grid points takes less computation time but the deviation is more than 7%. Hence, the grid system with 10,251 grid points is selected as a typical grid and all other computations are carried out using this grid system.

## 4 Experimental work

Experiments were conducted on a specially designed roll coating machine for laboratory experiments. The laboratory coater consists of two equal rolls of 150mm radii and a big roll of 500mm radius. All three rolls are horizontally mounted; polished, hard chrome plated steel rolls with 300mm length each. The schematic diagram of the experimental

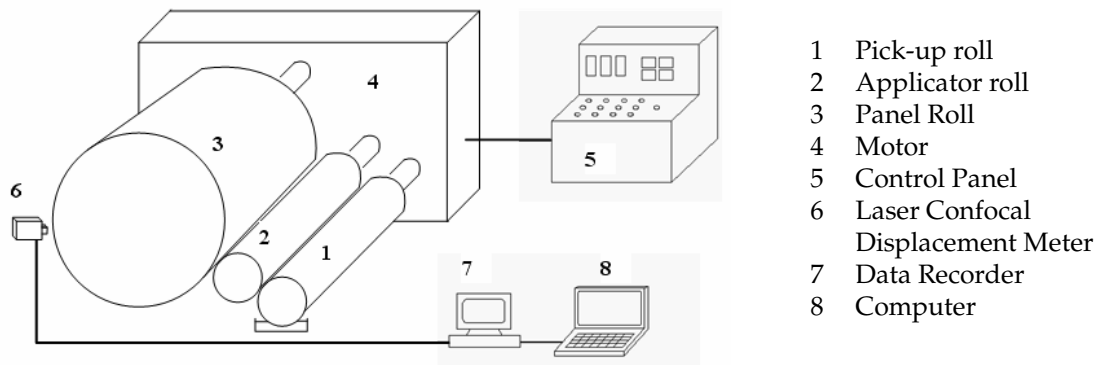


Figure 5: Schematic diagram of the experimental setup.

coating system is shown in Fig. 5. All rolls are driven by three separate motors with feed back control system. A polymer powder non-Newtonian solution was used in the experiments.

The applicator roll and pickup rolls are arranged horizontally and are half submerged in a bath of coating liquid i.e. enamel pan. The pick up roll dips in enamel pan and picks up the coating liquid and then forms a liquid film while rotating with applicator roll in same direction. The gap between the two reverse rolls is of the order of magnitude of  $25 \mu\text{m}$ . The thickness of arriving liquid film is maintained as 100 microns. The rotational speeds of the rolls were detected by the two digital tachometers attached to the rolls. Rolls can rotate up to a maximum speed of 10 m/s. Applicator roll speed is maintained at 4 m/s while panel roll or back up roll speed varied as 2 m/s, 4m/s and 8 m/s order to give to different speed ratios.

The film thickness is measured by adopting high accuracy surface scanning laser confocal displacement meter (LT-9001 by Keyence Corporation). This sensor works on confocal principle and gives an excellent resolution of  $0.3 \mu\text{m}$ . The data from the sensor is recorded using data recorder in order to send the collected data to laptop computer for further analysis. Experiments were carried out by considering different values of speed ratios and nip gap distance.

## 5 Results and discussion

Computations were performed on an Intel Xeon 3.4 workstation with 3.4GHz CPU. The typical CPU times were 15 hours for solving one non-Newtonian case. Figs. 6 and 7 present the velocity vector plots, film thickness, respectively, affected by roll speed ratio ( $V_2/V_1=0.5, 1.0$  and  $2.0$ , where  $V_2$  and  $V_1$  are surface speed panel roll and applicator roll, respectively) with gap =  $25\mu\text{m}$ ,  $\mu_0 = 4.5 \times 10^{-3}\text{Pa}\cdot\text{s}$  ( $n = 0.95$ ) and  $\sigma = 0.028 \text{ N/m}$ . It is noted that the applicator roll speed is maintained at 4 m/s. The conservation of volume

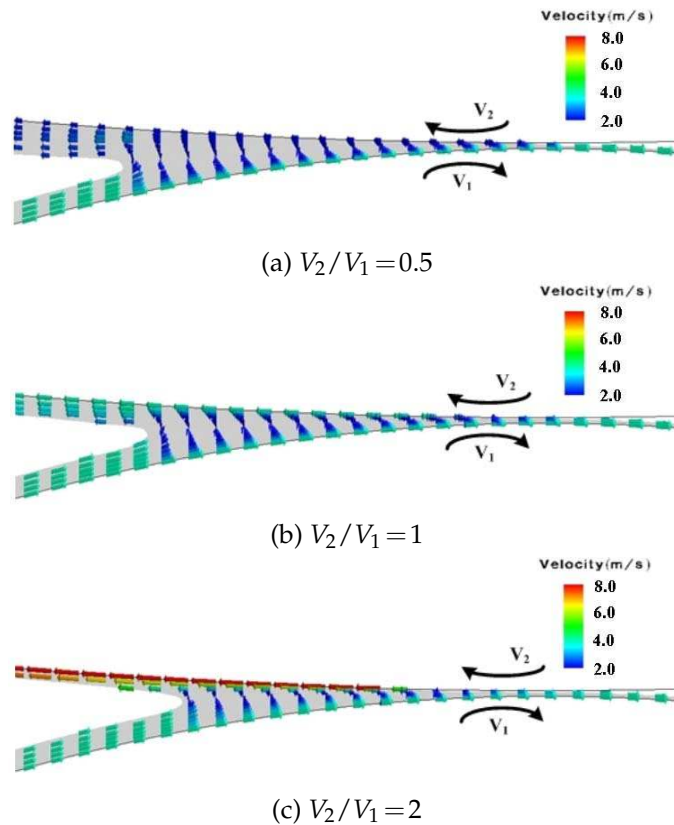


Figure 6: Velocity vector plots for different speed ratios with the gap =  $25\mu\text{m}$ ,  $\mu_0 = 4.5 \text{ m Pa-s}$  ( $n = 0.95$ ) and  $\sigma = 0.028 \text{ N/m}$ .

flow rate near the nip gap region can be verified by using following equation:

$$\left( \int_0^t lV \cdot \hat{n} dy \right)_{inlet} = \left( \int_0^t lV \cdot \hat{n} dy \right)_{transferred} + \left( \int_0^t lV \cdot \hat{n} dy \right)_{leakage}, \quad (5.1)$$

where  $t$ ,  $l$  and  $V$  is coating film thickness, length of rolls and local velocity of fluids, respectively. As expectedly, the flow fields are significantly affected by the speed ratio. As the roll speed ratio ( $V_2/V_1$ ) is increased, the transferred film thickness ( $t_2$ ) is reduced and the upstream film splitting point is getting closer to the nip gap. The reason is that increasing the speed ratio ( $V_2/V_1$ ) pulls the wetting line through the gap and causes the recirculation to shrink. It is also observed that the thickness of leakage fluid film ( $t_3$ ), which returns back to the enamel pan, is increased as raising the roll speed ratio. It is seen that the transferred film thickness is reduced about 74%, but the leakage film thickness is increased about 12% as the roll speed ratio ( $V_2/V_1$ ) is increased from 0.5 to 2.

Fig. 8 shows the variation of fluid pressure profiles for different speed ratio ( $V_2/V_1$ ) between two rollers. It is seen from pressure profiles that the maximum positive peak

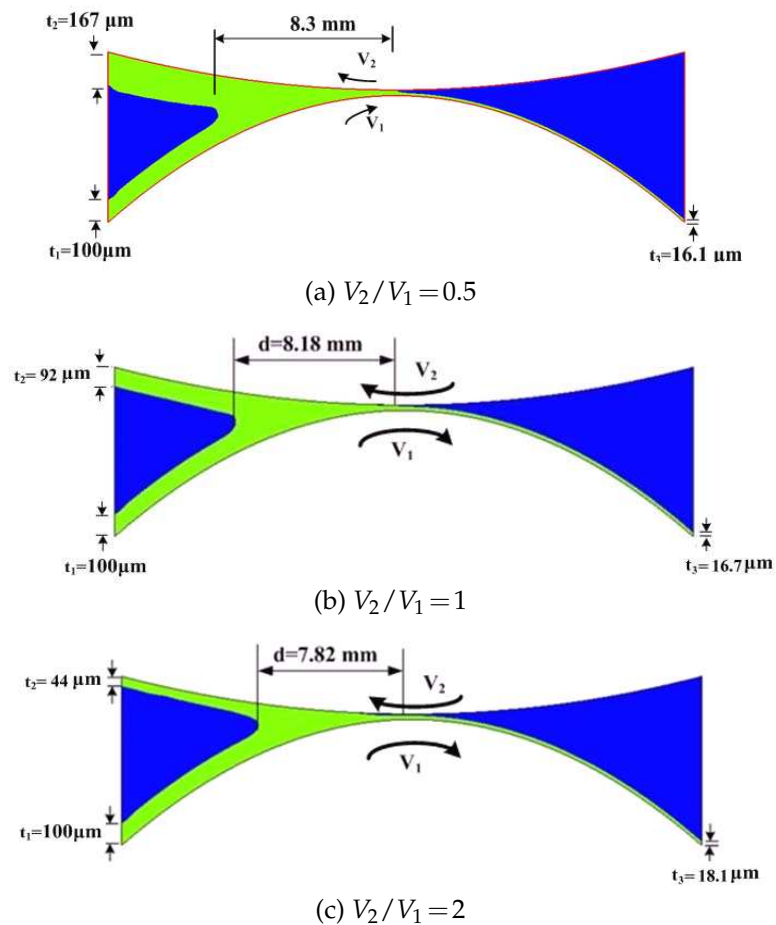


Figure 7: Effect of speed ratio on transferred and leakage film thicknesses with gap =  $25\mu\text{m}$ ,  $\mu = 4.5 \text{ m Pa}\cdot\text{s}$  ( $n = 0.95$ ) and  $\sigma = 0.028 \text{ N/m}$ .

pressure is obtained for roll speed ratio of 0.5. Positive peak pressure is attained gradually as the speed ratio is decreased, while negative peak pressure is archived almost instantaneously near the nip point, and minimum negative peak pressure is obtained for roll speed ratio of 2. It is seen that maximum positive peak pressure is reduced about 68% as the roll speed ratio  $V_2/V_1$  is increased from 0.5 to 1.0, while the minimum negative peak pressure is increased about 37% as the roll speed ratio is increased from 1.0 to 2.0

Fig. 9 compares the transferred film thickness values obtained from both the numerical simulations and experiments with the gap =  $25\mu\text{m}$ ,  $\mu_0 = 4.5 \text{ m Pa}\cdot\text{s}$  ( $n = 0.95$ ) and  $\sigma = 0.028 \text{ N/m}$ . The trend in both experimental curve and numerical data curve is similar. The numerical results underpredict the transferred film thickness against the experimental values and the error between the numerical and experimental data is within 15-20%. This deviation may come from machining vibration.

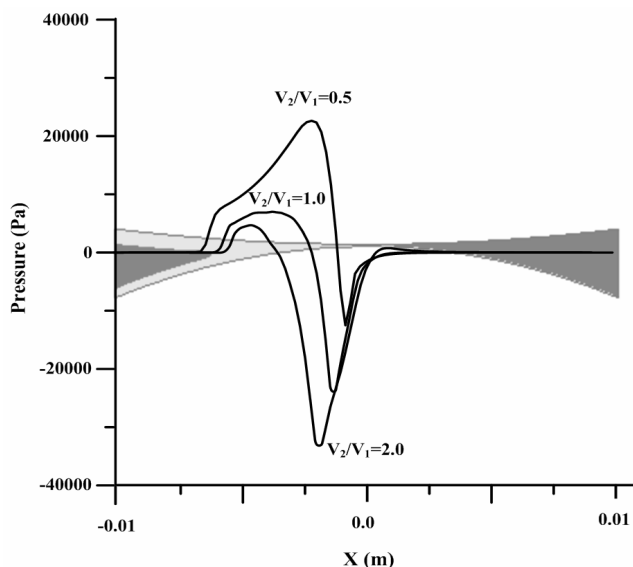


Figure 8: Effect of speed ratio on gauge pressure with gap =  $25\mu\text{m}$ ,  $\mu_0 = 4.5\text{ m Pa-s}$  ( $n = 0.95$ ), and  $\sigma = 0.028\text{ N/m}$ .

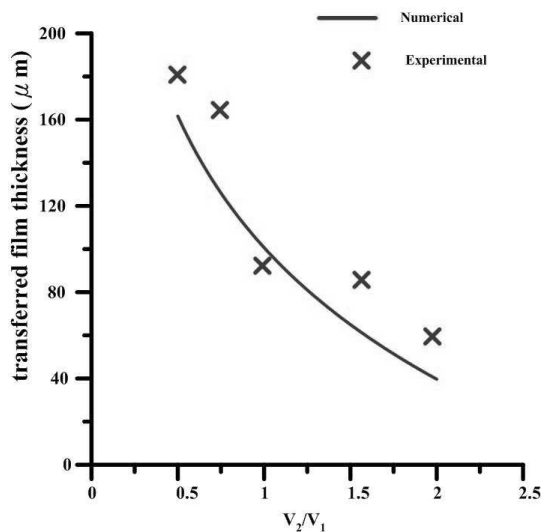


Figure 9: Comparison of transferred film thickness against speed ratio with the gap =  $25\mu\text{m}$ ,  $\mu_0 = 4.5\text{ m Pa-s}$  ( $n = 0.95$ ) and,  $\sigma = 0.028\text{ N/m}$ .

The effect of nip gap distance between reverse rolls on the transferred and leakage film thicknesses is shown in Fig. 10. Three different values of  $0\mu\text{m}$ ,  $25\mu\text{m}$  and  $50\mu\text{m}$  are considered with  $V_2/V_1 = 0.5$ ,  $\mu_0 = 4.5\text{ mPa-s}$  ( $n = 0.95$ ), and  $\sigma = 0.028\text{ N/m}$  in numerical computations. Results indicate that transferred film thickness is reduced 17% for the increase in nip gap distance from  $25\mu\text{m}$  to  $50\mu\text{m}$  and more film leakage is caused.

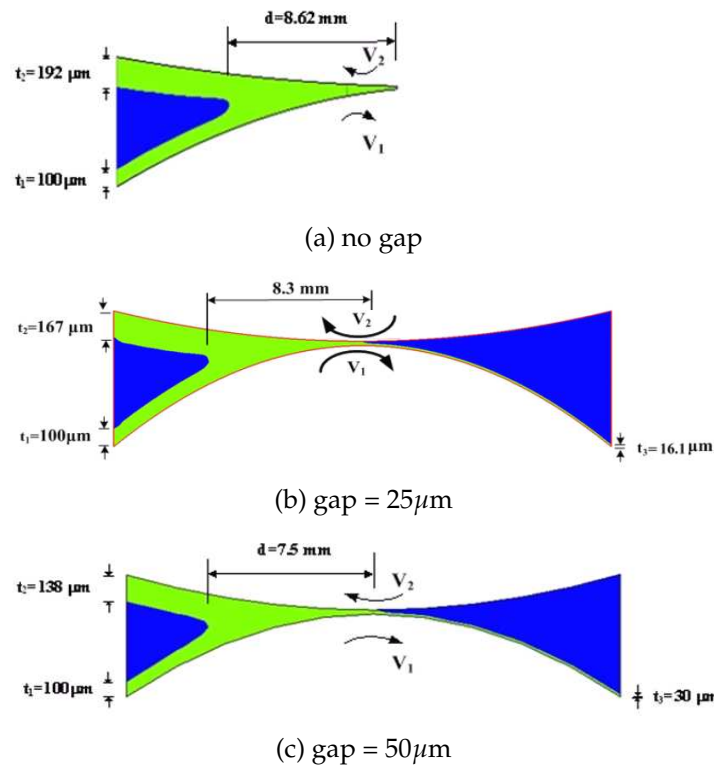


Figure 10: Effect of gap distance on transferred and leakage film thicknesses with  $V_2/V_1 = 0.5$ ,  $\mu_0 = 4.5 \text{ mPa}\cdot\text{s}$  ( $n = 0.95$ ), and  $\sigma = 0.028 \text{ N/m}$ .

Effect of gap distance on gauge pressure with  $V_2/V_1 = 0.5$ ,  $\mu_0 = 4.5 \text{ mPa}\cdot\text{s}$  ( $n = 0.95$ ), and  $\sigma = 0.028 \text{ N/m}$  is shown in Fig. 11. Three gap distances of  $0\mu\text{m}$ ,  $25\mu\text{m}$  and  $50\mu\text{m}$  between two rolls are considered in the present study. Pressure values are plotted against upstream side distance from gap center ( $x$ ) between rolls. As expectedly, the lower the gap distance, the higher the pressure peak. Maximum peak gage pressure value of 130 KPa is observed when there is no gap between the rolls. And as the gap distance is increased from  $25\mu\text{m}$  to  $50\mu\text{m}$ , the maximum peak pressure is decreased from 22.5 KPa to 16.8 KPa.

Fig. 12 shows the effect of power index  $n$  ( $n = 0.8, 0.95$ , and  $1.2$ ) on the transferred and leakage film thickness with the gap =  $25\mu\text{m}$ ,  $V_2/V_1 = 0.5$ ,  $\mu_0 = 4.5 \text{ mPa}\cdot\text{s}$ , and  $\sigma = 0.028 \text{ N/m}$ . It is observed that as the power index  $n$  is increased, the transferred film thickness is increased, while the leakage film thickness is decreased and the film splitting point moves further away from the gap between two rolls. The transferred film thickness is increased about 15%, but the leakage film thickness is decreased about 14% as the power index  $n$  is increased from 0.8 to 1.2.

Fig. 13 shows the effect of power indices  $n$  ( $n = 0.8, 0.95$  and  $1.2$ ) on gauge pressure with the gap =  $25\mu\text{m}$ ,  $V_2/V_1 = 0.5$ ,  $\mu_0 = 4.5 \text{ mPa}\cdot\text{s}$ , and  $\sigma = 0.028 \text{ N/m}$ . Pressure values

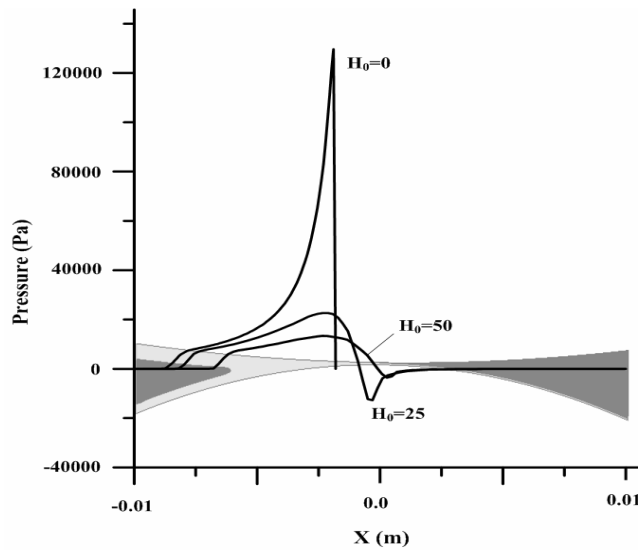


Figure 11: Effect of gap distance on gauge pressure with  $V_2/V_1=0.5$ ,  $\mu_0=4.5$  mPa-s ( $n=0.95$ ), and  $\sigma=0.028$  N/m.

are plotted against film splitting point distance ( $x$ ) at nip point. It is seen that maximum positive peak pressure and minimum negative peak pressure are obtained for  $n = 1.2$ . All the three coating fluids attain maximum positive peak values at nearly same values of  $x$ . The maximum positive peak pressure and minimum negative peak pressure are increased about two times as increasing the power index  $n$  from 0.8 to 1.2. Effect of power-law index  $n$  and roll speed ratio on film thickness ratio with the gap =  $25\mu\text{m}$ ,  $\mu_0 = 4.5$  m Pa-s, and  $\sigma = 0.028$  N/m is shown in Fig. 14. It is seen that the film thickness ratio  $t_2/t_1$  is decreased, while  $t_3/t_1$  is slightly increased with increasing the roll speed ratio. The effect of power-law index  $n$  for thickness ratio of  $t_2/t_1$  is more obvious than  $t_3/t_1$ .

Fig. 15 demonstrates the effect of power index  $n$  and gap on film thickness ratio with  $V_2/V_1 = 0.5$ ,  $\mu_0 = 4.5$  m Pa-s, and  $\sigma = 0.028$  N/m. It is shown that the film thickness ratio  $t_2/t_1$  is increased, while  $t_3/t_1$  is decreased with raising the power index  $n$ , and for ratio of  $t_2/t_1$  or  $t_3/t_1$ , the difference is about 15.8% to 85.5% as  $H_0/R_m$  is raised from  $7.7 \times 10^{-5}$  to  $1.54 \times 10^{-4}$ , where  $R_m$  is average radius of two rolls and  $H_0$  is gap distance. From Figs. 14-15, it would be useful if the results of transferred and leakage film thicknesses can be presented in the following simple correlations:

$$\frac{t_2}{t_1} = 0.89n^{0.55} \left(\frac{V_2}{V_1}\right)^{-0.83} \left(\frac{H_0}{R_m}\right)^{0.0025}, \quad (5.2)$$

$$\frac{t_3}{t_1} = 65.6n^{0.0014} \left(\frac{V_2}{V_1}\right)^{-0.043} \left(\frac{H_0}{R_m}\right)^{0.624}, \quad (5.3)$$

where  $t_1$ ,  $t_2$  and  $t_3$  are inlet film, transferred film and leakage film thickness, respectively,

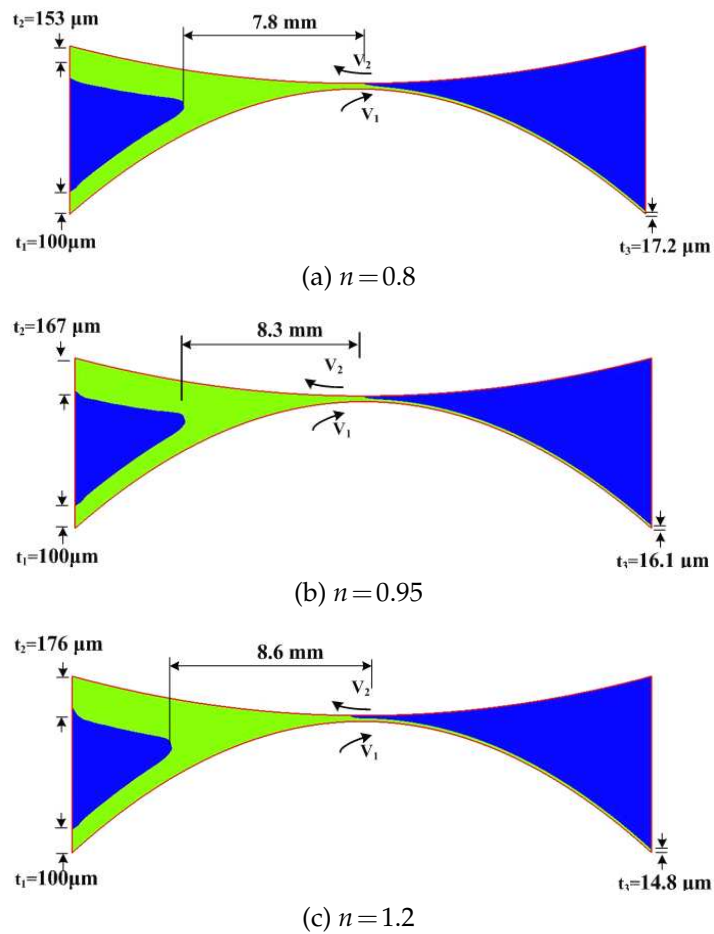


Figure 12: Effect of power index  $n$  on transferred and leakage film thicknesses with the gap =  $25\mu\text{m}$ ,  $V_2/V_1=0.5$ ,  $\mu_0=4.5\text{ m Pa}\cdot\text{s}$ , and  $\sigma=0.028\text{ N/m}$ .

$n$  is power-law index,  $V_1$  and  $V_2$  are roll speed of applicator roll and panel roll,  $R_m$  is average radius of two rolls and  $H_0$  is gap distance. The above correlations were obtained by a regression analysis, which are accurate within 10% for  $0.8 \leq n \leq 1.2$ ,  $0.5 \leq V_2/V_1 \leq 2$ , and  $7.7 \times 10^{-5} \leq H_0/R_m \leq 1.54 \times 10^{-4}$ . It should be noted that the gravity in numerical simulation is ignored because the gap is very small compared to radius of roll, that is  $H_0/R \ll 1$ . For large gap distance the effect of gravity should be taken into account to predict the film thickness ratio more exactly (Gaskell, Innes and Savage [15]).

## 6 Conclusion

An attempt had been made to analyze numerically and experimentally the two dimensional non-Newtonian flow between two rolls of a reverse roll coating process. The non-

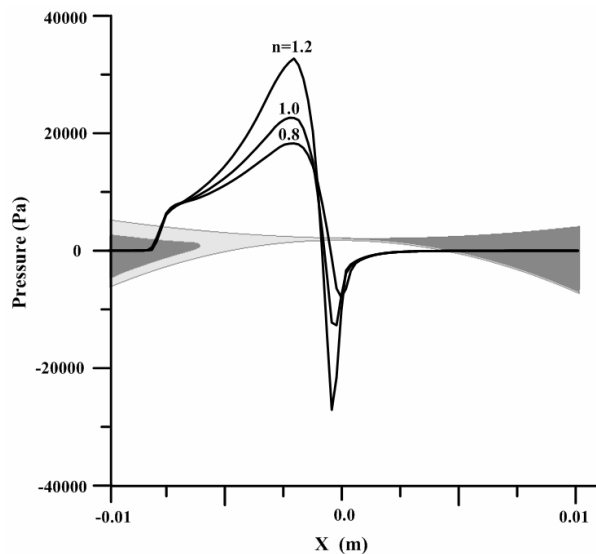


Figure 13: Effect of power index  $n$  on gauge pressure with the gap =  $25\mu\text{m}$ ,  $V_2/V_1=0.5$ ,  $\mu_0=4.5\text{ m Pa-s}$ , and  $\sigma=0.028\text{ N/m}$ .

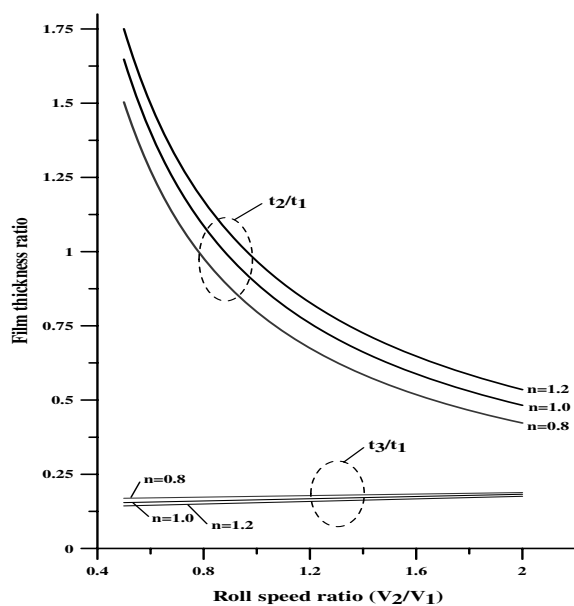
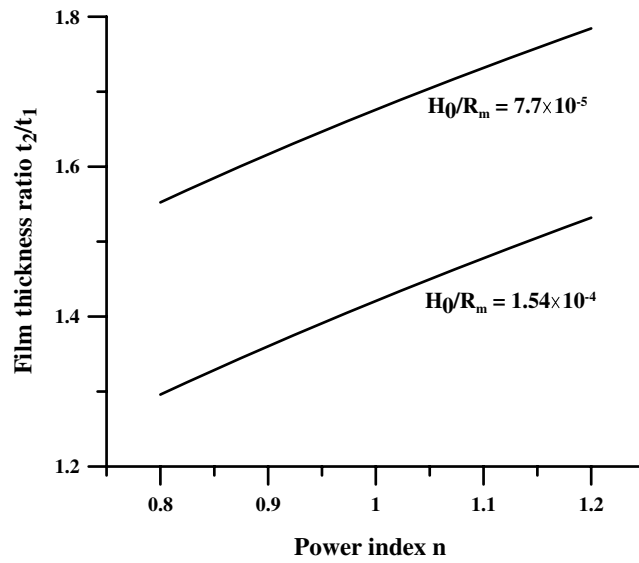
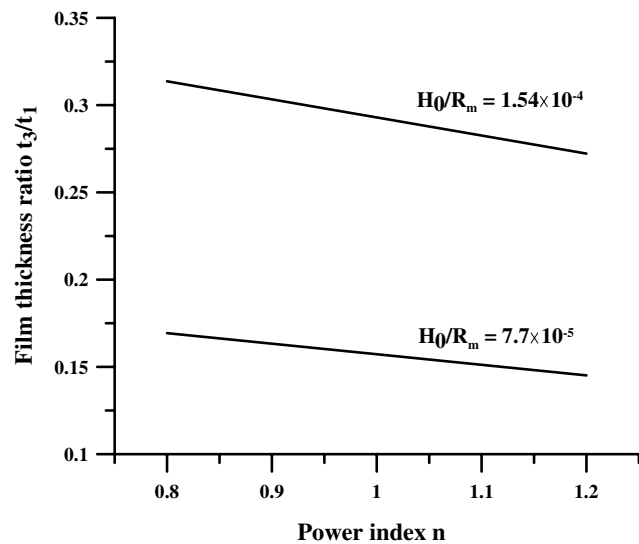


Figure 14: Effect of power index  $n$  and roll speed ratio on film thickness ratio with the gap =  $25\mu\text{m}$ ,  $\mu_0=4.5\text{ m Pa-s}$ , and  $\sigma=0.028\text{ N/m}$ .

Newtonian behavior of the coating fluid had also been accounted using Ostwald's power law model with power index values of  $n$  ranging from 0.8 to 1.2. The agreement between the numerical results and measured data is within 15-20%. It is found that, as either the



(a) Variation of film thickness ratio  $t_2/t_1$  with power index and  $H_0/R_m$



(b) Variation of film thickness ratio  $t_3/t_1$  with power index and  $H_0/R_m$

Figure 15: Effect of power index  $n$  and gap on film thickness ratio with  $V_2/V_1 = 0.5$ ,  $\mu_0 = 4.5$  m Pa-s, and  $\sigma = 0.028$  N/m.

speed ratio ( $V_2/V_1$ ) or the gap distance is increased, the transferred film thickness is reduced, while the leakage film thickness is increased. As the power index is increased, the transferred film thickness is increased, while the leakage film thickness is decreased and the film splitting point moves further away from the gap centre between two rolls. Two

correlations for the transferred and leakage film thickness ratios are obtained and the accuracy is within 10% for  $0.8 \leq n \leq 1.2$ ,  $0.5 \leq V_2/V_1 \leq 2$ , and  $7.7 \times 10^{-5} \leq H_0/R_m \leq 1.54 \times 10^{-4}$ .

## Acknowledgments

Authors acknowledge the financial and experimental support provided by China Steel Corporation, Kaohsiung, Taiwan and also Dr. Venkatesh M. Kulkarni for his help in preparing the manuscript.

## References

- [1] G.L. Booth, *Coating Equipment and Processes*, New York: Lockwood Publishing Company. (1970)
- [2] D.G. Higgins, *Coating methods-survey*, *Encyclopedia of Polymer Science and Technology*, 3 (1965), 765-807.
- [3] W.S. Ho and F.M. Holland, *Between roll metering coating technique – A theoretical and experiment study*, *TAPPI Journal*, 61 (1978), 53-56.
- [4] J. Greener and S. Middleman, *Reverse roll coating of viscous and viscoelastic liquids*, *Ind. Eng. Chem. Fundam.*, 20 (1981), 63-66
- [5] D.J. Coyle, C.W. Macosko and L.E. Scriven, *The fluid dynamics of reverse roll coating*, *AIChE Journal*, 36 (1990), 161-174.
- [6] D.J. Coyle, C.W. Macosko and L.E. Scriven, *A simple model of reverse rolls coating*, *Ind. Eng. Chem. Res.*, 29 (1990), 1416-1419.
- [7] Y. Hao and S. Haber, *Reverse roll coating flow*, *Int. J. Numer. Meth. Fluids*, 30 (1999), 635-652.
- [8] M.S. Chandio and M.F. Webster, *Numerical simulation for reverse roller coating with free surfaces*, *ECCOMAS Computational Fluid Dynamics Conference*, UK: Swansea, 4-7 September, (2001), 1-11.
- [9] M.S. Chandio and M.F. Webster, *Numerical simulation for viscous free-surface flows for reverse roller-coating*, *Int. J. Numer. Meth. Heat Fluid Flow*, 12-4 (2002), 434-457.
- [10] D.J. Coyle, C.W. Macosko and L.E. Striven, *Reverse roll coating of non-Newtonian liquids*, *J. Rheology*, 34-5 (1990), 615-636.
- [11] C. Tiu, L. Wang and T.J. Liu, *Non-Newtonian effects on pre-metered reverse roll coating*, *J. Non-Newtonian Fluid Mech.*, 87 (1999), 247-261.
- [12] W.L. Wilkinson, *Non-Newtonian Fluids – Fluids Mechanics, Mixing and Heat Transfer*, Pergamon, New York, (1960).
- [13] C.W. Hirt and B.D. Nichols, *Volume of fluid method for the dynamics of free boundaries*, *J. Comput. Phys.*, 39 (1981), 210-225.
- [14] S.V. Patankar, *Numerical Heat Transfer and Fluid Flow*, Hemisphere Publishing Corporation, (1984).
- [15] P.H. Gaskell, G.E. Innes and M.D. Savage, *An experimental investigation of meniscus roll coating*, *J. Fluid Mech.*, 355 (1998), 17-44.